Journal of Power Sources 192 (2009) 267–278

Contents lists available at ScienceDirect

Journal of Power Sources

journal homepage: www.elsevier.com/locate/jpowsour

Measurement of oxygen chemical potential in Gd_2O_3-doped ceria-Y_2O_3-stabilized zirconia bi-layer electrolyte, anode-supported solid oxide fuel cells

Hyung-Tae Lim, Anil V. Virkar*

Department of Materials Science and Engineering, 122 S. Central Campus Drive, University of Utah, Salt Lake City, UT 84112, United States

ARTICLE INFO

Article history:
Received 12 February 2009
Received in revised form 17 March 2009
Accepted 18 March 2009
Available online 27 March 2009

Keywords:
Ceria
Zirconia
Bi-layer
Solid oxide fuel cells
Oxygen chemical potential

ABSTRACT

Solid oxide fuel cells (SOFC) were fabricated with gadolinia-doped ceria (GDC)–yttria stabilized zirconia (YSZ), thin bi-layer electrolytes supported on Ni + YSZ anodes. The GDC and YSZ layer thicknesses were 45 μm, and ~5 μm, respectively. Two types of cells were made; YSZ layer between anode and GDC (GDC/YSZ) and YSZ layer between cathode and GDC (YSZ/GDC). Two platinum reference electrodes were embedded within the GDC layer. Cells were tested at 650 °C with hydrogen as fuel and air as oxidant. Electric potentials between embedded reference electrodes and anode and between cathode and anode were measured at open circuit, short circuit and under load. The electric potential was nearly constant through GDC in the cathode/YSZ/GDC/anode cells. By contrast, it varied monotonically through GDC in the cathode/GDC/YSZ/anode cells. Estimates of oxygen chemical potential, μ_{O_2}, variation through GDC were made. μ_{O_2} within the GDC layer in the cathode/GDC/YSZ/anode cell decreased as the current was increased. By contrast, μ_{O_2} within the GDC layer in the cathode/YSZ/GDC/anode cell increased as the current was increased. The cathode/YSZ/GDC/anode cell exhibited maximum power density of ~0.52 W cm^{-2} at 650 °C while the cathode/GDC/YSZ/anode cell exhibited maximum power density of ~0.14 W cm^{-2} for the same total electrolyte thickness.

1. Introduction

The most commonly used solid electrolyte in anode-supported solid oxide fuel cells (SOFC) is yttria-stabilized zirconia (YSZ), which is a predominantly oxygen ion conductor with negligible electronic conductivity. Typical operating temperature for SOFC with YSZ electrolyte is above 750 °C. There is also considerable interest in rare earth oxide doped ceria (RDC), such as Sm_2O_3-doped CeO_2 (SDC) and Gd_2O_3-doped CeO_2 (GDC), as electrolyte because of its higher oxygen ion conductivity than YSZ, which allows operation at lower temperatures—down to about 600 °C. Both GDC and SDC (and other rare earth oxide doped ceria or RDC) exhibit mixed ionic electronic conduction (MIEC), especially in reducing atmospheres. Thus, the open circuit voltage (OCV) with ceria as the electrolyte is typically lower than the corresponding Nernst voltage. At an operating temperature of ~650 °C, the OCV with ceria-based cells is typically ~0.8 V with hydrogen/air, which results in a significant penalty concerning fuel cell efficiency. A potential solution is the use of a bi-layer electrolyte, comprising an RDC electrolyte with a thin YSZ layer [1–12]. The thin YSZ layer then can essentially block off the electronic current and raise the OCV. At the same time, as the YSZ layer is thin, the increase in ionic resistance is rather modest. Such a bi-layer electrolyte thus in principle can achieve not only a lower temperature operation (due to higher oxygen ion conductivity) but also increase the OCV due to the blockage of electronic current by the thin YSZ layer.

Although the electronic conductivity of ceria increases in a reducing atmosphere, it remains chemically, physically, and structurally stable over a wide range of oxygen partial pressures. Thus, in bi-layer cells, the main function of YSZ is to block off the electronic current. For blocking the electronic current, the YSZ layer may be placed either between the cathode and the electrolyte, or between the anode and the electrolyte.[1] Although the purpose of the YSZ layer is clear, it is not obvious what the location of the YSZ layer should be; whether between the RDC and the cathode or between the RDC and the anode. Also, even if the YSZ may remain a predominantly ionic conductor at either location, the variations in chemical potential of oxygen and electric potential through the RDC electrolyte will in general be different for the two different locations of the YSZ thin layer. The objective of the present work was to experimentally evaluate these two different bi-layer elec-

* Corresponding author.
E-mail address: anil.virkar@m.cc.utah.edu (A.V. Virkar).

[1] By contrast, if bismuth oxide is used as the electrolyte, the YSZ layer must be between the anode and the electrolyte otherwise bismuth oxide will readily decompose in hydrogen. It is to be emphasized that bismuth oxide may decompose even with a YSZ layer on the anode side, depending upon transport properties.

0378-7753/$ – see front matter © 2009 Elsevier B.V. All rights reserved.
doi:10.1016/j.jpowsour.2009.03.035

Nomenclature

E	Nernst voltage (V)
E_M	open circuit voltage (V)
$I_{O^{2-}}$	oxygen ion current density (A cm^{-2})
I_e	electronic current density (A cm^{-2})
x	distance (cm)
e	electronic charge (coulombs)
k_B	Boltzmann constant
p_{O_2}	oxygen partial pressure
$p^c_{O_2}$	oxygen partial pressure in the electrolyte just inside the cathode/electrolyte interface
$p^a_{O_2}$	oxygen partial pressure in the electrolyte just inside the anode/electrolyte interface
$p^I_{O_2}$	oxygen partial pressure in the cathode gas
$p^{II}_{O_2}$	oxygen partial pressure in the anode gas
T	temperature (K)
r^c_i	cathode/electrolyte ionic area specific resistance (Ω cm^2)
r^{YSZ}_i	ionic area specific resistance of the YSZ layer (Ω cm^2)
r^{GDC}_i	ionic area specific resistance of the GDC layer (Ω cm^2)
$r^{el}_i = r^{YSZ}_i + r^{GDC}_i$	electrolyte ionic area specific resistance (Ω cm^2)
r^a_i	anode/electrolyte ionic area specific resistance (Ω cm^2)
r^c_e	cathode/electrolyte electronic area specific resistance (Ω cm^2)
r^{YSZ}_e	electronic area specific resistance of the YSZ layer (Ω cm^2)
r^{GDC}_e	electronic area specific resistance of the GDC layer (Ω cm^2)
$r^{el}_e = r^{YSZ}_e + r^{GDC}_e$	electrolyte electronic area specific resistance (Ω cm^2)
r^a_e	anode/electrolyte electronic area specific resistance (Ω cm^2)
$R_i = r^c_i + r^{el}_i + r^a_i$	ionic area specific resistance of the membrane (Ω cm^2)
$R_e = r^c_e + r^{el}_e + r^a_e$	electronic area specific resistance of the membrane (Ω cm^2)
$t_i = R_e/(R_i + R_e)$	ionic transference number of the membrane including interfaces

Greek letters

μ_e	chemical potential of electrons
μ_h	chemical potential of holes
μ_{O_2}	chemical potential of oxygen
$\mu^c_{O_2}$	chemical potential of oxygen in the electrolyte just inside the cathode/electrolyte interface
$\mu^a_{O_2}$	chemical potential of oxygen in the electrolyte just inside the anode/electrolyte interface
$\mu^I_{O_2}$	chemical potential of oxygen in the cathode gas
$\mu^{II}_{O_2}$	chemical potential of oxygen in the anode gas
$\tilde{\mu}_{O^{2-}}$	electrochemical potential of oxygen ions
$\tilde{\mu}_e$	electrochemical potential of electrons
$\varphi = -\tilde{\mu}_e/e$	reduced negative electrochemical potential of electrons or electric potential (V)
Φ	electrostatic potential (V)
$\sigma_{O^{2-}}$	oxygen ion conductivity (S cm^{-1})
σ_e	electronic conductivity (S cm^{-1})

trolyte configurations from the standpoint of spatial variation of oxygen chemical potential, μ_{O_2}, and performance.

The variation of μ_{O_2} through mixed ionic and electronic conducting (MIEC) materials has been numerically estimated by several authors [13–18] using the approach described by Wagner many years ago [19]. The approach consists of solving the transport equations by taking into account the flux of oxygen ions (typically by a vacancy mechanism) and of electrons (and/or holes) under imposed experimental conditions. The ionic and electronic current densities are given by

$$I_{O^{2-}} = -\frac{\sigma_{O^{2-}}}{2e}(-\nabla\tilde{\mu}_{O^{2-}}) \quad I_e = -\frac{\sigma_e}{e}(-\nabla\tilde{\mu}_e) \tag{1}$$

where the ionic conductivity, $\sigma_{O^{2-}}$, and the electronic conductivity, σ_e, may depend upon μ_{O_2}, which may be position-dependent; $\tilde{\mu}_{O^{2-}}$ and $\mu_{O^{2-}}$ are electrochemical potential and chemical potential of oxygen ion, respectively, where $\tilde{\mu}_{O^{2-}} = \mu_{O^{2-}} - 2e\Phi$; $\tilde{\mu}_e$ and μ_e are electrochemical potential and chemical potential of electrons, respectively, where $\tilde{\mu}_e = \mu_e - e\Phi$, e is the electronic charge, and Φ is the local electrostatic potential (as defined by Coulomb's law). Local equilibrium gives $\tilde{\mu}_{O^{2-}} = (1/2)\mu_{O_2} + 2\tilde{\mu}_e$. The equilibration of oxygen chemical potential, μ_{O_2}, across gas–solid interfaces is usually assumed. Under this situation, it can be shown that

$$\mu_{O_2}(x) = \mu^I_{O_2} + 4e(I_{O^{2-}} + I_e)\int_0^x \frac{dx}{\sigma_{O^{2-}}(x)} + 4e\int_{\varphi^I}^{\varphi(x)} \left(\frac{\sigma_{O^{2-}}(x) + \sigma_e(x)}{\sigma_{O^{2-}}(x)}\right) d\varphi(x) \tag{2}$$

where $\varphi = -\tilde{\mu}_e/e$ is the reduced negative electrochemical potential of electrons (or reduced electrochemical potential of holes, $\varphi = \tilde{\mu}_h/e$) or electric potential. There are many such calculations reported in the literature [13–18]. However, no clear justification for the assumption concerning the equilibration of μ_{O_2} across both gas/solid interfaces has been provided. Also, numerical results given are based on experimental studies conducted with measurements made outside of the membrane, such as current or voltage measurements, and not probing the interior regions of the membrane. From these measurements and the assumption concerning μ_{O_2} equilibration across interfaces, the spatial variation of μ_{O_2} is deduced. The only experimental studies on the measurement of μ_{O_2} inside an oxygen transporting MIEC reported to the authors' knowledge are by Mineshige et al. [20] and by the present authors [21]. Mineshige et al. determined the spatial variation of μ_{O_2} by subjecting an RDC disc to different oxygen pressures at the two surfaces followed by a Raman spectroscopic study through the thickness [20].

The present authors used an embedded reference electrodes method to estimate the μ_{O_2} in a GDC electrolyte of an anode-supported SOFC [21]. Up to three platinum reference electrodes were embedded in a thin (~45 μm) GDC electrolyte. The reference electrodes were sealed off from the atmosphere using an oxygen impermeable glass. Thus, no exchange of oxygen could occur at the reference electrodes, and the measurements yield the electrochemical potential of electrons, $\tilde{\mu}_e$, or more specifically the negative of the reduced electrochemical potential of electrons (electric potential), φ. From these measurements, the μ_{O_2} variation through the GDC electrolyte was estimated. The results showed that the μ_{O_2} across the anode/electrolyte interface equilibrated—that is the μ_{O_2} in the gas phase at the anode was essentially the same as that within the electrolyte just across the anode/electrolyte interface. Also, the μ_{O_2} varied gradually throughout the GDC electrolyte, but exhibited a sharp change across the cathode/electrolyte interface. That is, the results showed that the μ_{O_2} did not equilibrate across the cathode/electrolyte interface. These results are in agreement with the experimental observations by Mineshige et al., who as stated before, used a Raman spectroscopic technique [20].

In the present work, anode-supported cells comprising GDC-YSZ bi-layer electrolyte were made. The YSZ layer was positioned between the anode and the GDC electrolyte in one set of cells (cathode/GDC/YSZ/anode), and between the cathode and the GDC electrolyte in the other set of cells (cathode/YSZ/GDC/anode). Two reference electrodes were embedded within the GDC electrolyte layer. The cells were tested under OCV, under short circuit and under various loads at 650 °C with hydrogen as fuel and air as oxidant.

2. Experimental procedure

2.1. Cell fabrication

Anode-supported cells were fabricated using the following procedure. A powder mixture containing 70 wt.% NiO and 30 wt.% YSZ (composition: 8 mol.% Y_2O_3–92 mol.% ZrO_2) was made to which 10 wt.% carbon black was added to create porosity upon burn off. Ethylene glycol (6%) was added as a binder. Discs 3.3 cm in diameter and 1.5 mm in thickness were die-pressed at 26 MPa and fired at 950 °C in air for 1 h. Additional porosity was created in the anode upon subsequent reduction of NiO to Ni during cell testing. These discs were used as anode supports. Two types of cells with bi-layer GDC/YSZ electrolyte were made as described in what follows.

2.2. Set 1 (cathode/GDC/YSZ/anode)

A slurry containing 50 wt.% NiO and 50 wt.% YSZ (composition: 8 mol.% Y_2O_3–92 mol.% ZrO_2) was prepared in butyl alcohol. Anode functional layer was applied using the NiO + YSZ slurry on one side of an anode support disc by drop coating. The disc was fired at 950 °C for 1 h. Then, first a thin layer of YSZ was applied by drop coating on the anode functional layer. Thereafter, the first GDC (composition: 20 mol.% Gd_2O_3–80 mol.% CeO_2) electrolyte layer was drop-coated using GDC slurry followed by firing at 1050 °C for 2 h. Platinum paste was applied in the form of a thin and a very narrow strip over the electrolyte layer to form a reference electrode (Ref. #2). The sample was heated to 950 °C for 1 h to remove organics from the Pt paste. A second layer of GDC was drop-coated to cover most of the surface except for leaving a small part of the Pt strip exposed. The cell was again fired at 1050 °C for 2 h. Another reference electrode (Ref. #1) was similarly applied, followed by heating to 950 °C for 1 h. Finally, one more layer of GDC was drop-coated over most of the surface leaving small parts of both electrodes exposed. The cell was sintered at 1450 °C for 5 h. The total thickness of the GDC electrolyte was ~45 μm with the two reference electrodes positioned ~15 μm from the cathode/electrolyte and the GDC/YSZ interfaces, respectively. The YSZ layer thickness was ~5 μm. After sintering, a cathode functional layer containing a mixture of Sr-doped $LaCoO_3$ (LSC) and GDC was applied, followed by firing at 1100 °C for 1 h. A layer of LSC was then applied as a cathode current collector followed by again firing at 1100 °C for 1 h. Thus, the cell structure can be described as cathode/GDC/YSZ/anode. Pt wires were attached using a silver paste to the exposed parts of the embedded Pt reference electrodes (probes). Exposed parts of the Pt reference electrodes were also coated with a paste of an alkali silicate glass from Specialty Glass, Inc. in ethylene glycol. The cell was fired at 850 °C for 30 min to fuse the glass and isolate the exposed parts of the reference electrodes from air. This completes the cell fabrication procedure. Fig. 1(a) shows a schematic of the cell along with the position of reference electrodes.

2.3. Set 2 (cathode/YSZ/GDC/anode)

A slurry containing 50 wt.% NiO and 50 wt.% GDC was prepared in butyl alcohol. Anode functional layer was applied using the NiO + GDC slurry on one side of an anode support disc by drop coating. The disc was fired at 950 °C for 1 h. A GDC layer was applied on the anode support prior to the application of a YSZ layer. The procedure of applying GDC layers and embedding two platinum electrodes was similar. A thin layer of YSZ was applied by drop coating YSZ slurry over the GDC layer. The cell was sintered at 1450 °C

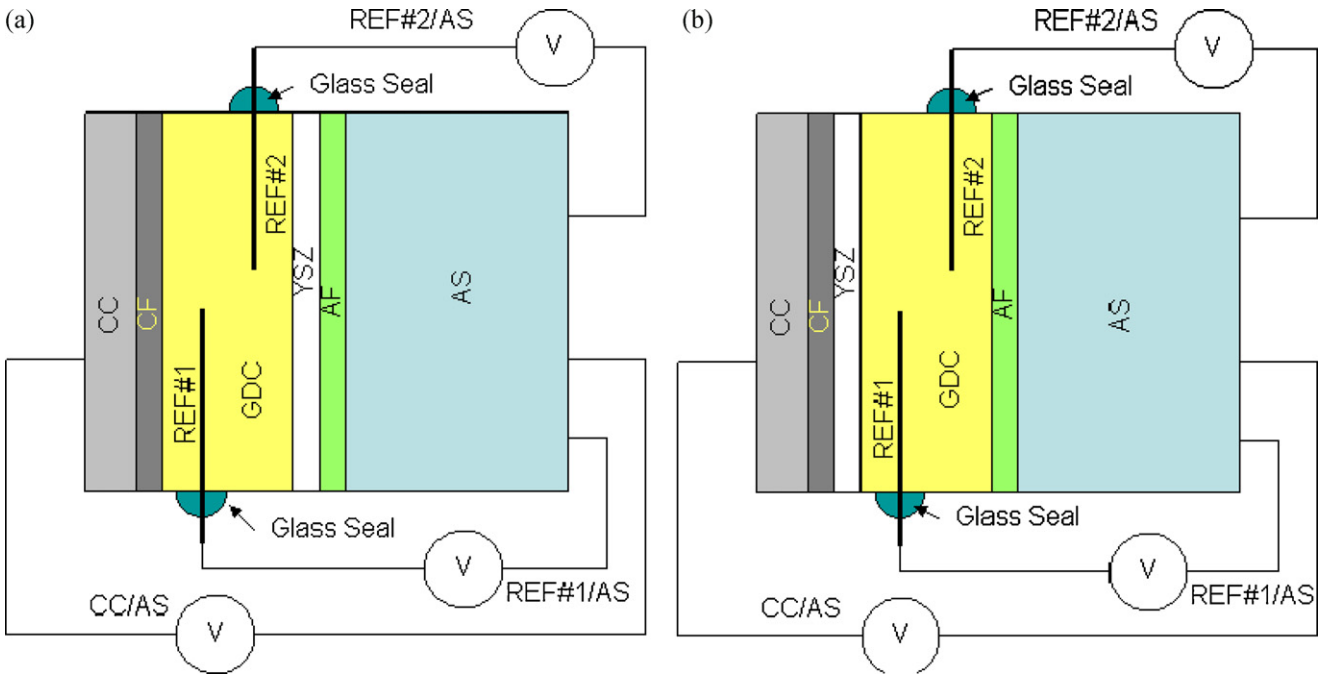

Fig. 1. (a) A schematic of an anode-supported cell with embedded reference electrodes in the GDC layer with the YSZ layer between the GDC and the anode interlayer or functional layer (AF). AS: anode support; CF: cathode interlayer or functional layer; CC: cathode current collector. (b) A schematic of an anode-supported cell with embedded reference electrodes in the GDC layer with the YSZ layer between the GDC and the cathode interlayer or functional layer (CF). AS: anode support; AF: anode interlayer or functional layer; CC: cathode current collector.

for 5 h. The total thickness of the GDC electrolyte was ~45 μm with the two reference electrodes positioned ~15 μm from the anode/electrolyte and the YSZ/GDC interfaces, respectively. The YSZ layer thickness was ~5 μm. After sintering, a cathode functional layer containing a mixture of Sr-doped $LaMnO_3$ (LSM) and YSZ was applied, followed by firing at 1170 °C for 1 h. A layer of LSM was then applied as a cathode current collector followed by again firing at 1150 °C for 1 h. The cell structure can be described as cathode/YSZ/GDC/anode. The procedure for the attachment of Pt wires and glass sealing was similar to Set 1. Fig. 1(b) shows a schematic of the cell along with the position of reference electrodes.

2.4. Cell testing

The following procedure was used for electrochemical testing of cells. For each test, a cell was secured in a test fixture using a mica gasket on the anode side as a seal. The cell was heated to 650 °C. Initially, a gas mixture containing 10% hydrogen + balance nitrogen at a flow rate of 300 ml min^{-1} was circulated past the anode and air at a flow rate of 300 ml min^{-1} past the cathode. After 4 h, the anode gas was switched to ~100% hydrogen. The voltages between the cathode and the anode and between the anode and the reference electrodes were initially measured under open circuit conditions. Subsequently, cell performance was measured over a range of loads from open circuit to short circuit conditions.

2.5. Measurement of ionic conductivity of GDC and YSZ in air

Bar-shaped samples of GDC and YSZ, with 3% ethylene glycol added as a binder, were made by die-pressing respective powders at 26 MPa followed by sintering at 1450 °C for 4 h. Platinum strips were painted on the bars in a four probe configuration. Samples were heated to 650 °C and four probe DC resistance was measured. Since the measurements were conducted in air at 650 °C, the predominant charge transport in both GDC and YSZ is by oxygen ions. From the sample dimensions, the corresponding ionic conductivities (resistivities) were estimated.

3. Results and discussion

3.1. Microstructure of Bi-layer cells with embedded reference electrodes

Fig. 2(a) and (b) is scanning electron micrograph (SEM) of a tested cell showing the LSC + GDC cathode interlayer, the GDC/YSZ electrolyte, and the Ni + YSZ anode interlayer. Fig. 3(a) and (b) is SEM micrograph of a tested cell showing the LSM + YSZ cathode interlayer, the YSZ/GDC electrolyte, and the Ni + GDC anode interlayer. In both cases, the GDC electrolyte thickness is ~45 μm while the YSZ layer thickness is ~5 μm. As seen in the micrographs, the two Pt reference electrodes are symmetrically embedded in the GDC layer. For the cathode/GDC/YSZ/anode cell for example, Ref. #1 (close to the cathode) and Ref. #2 (close to the anode) are ~15 μm from the cathode/electrolyte interface and ~15 μm from the GDC/YSZ interface, respectively. For the cathode/YSZ/GDC/anode cell, Ref. #1 (close to the cathode) and Ref. #2 (close to the anode) are ~15 μm from the YSZ/GDC interface and ~15 μm from the anode/electrolyte interface, respectively. Both the GDC/YSZ and the YSZ/GDC electrolyte appear to be dense with negligible porosity.

3.2. Chemical analysis of bi-layer cells

Fig. 4(a) and (b) shows EDAX scans on cathode/GDC/YSZ/anode and cathode/YSZ/GDC/anode cells. The beam size was 2 μm. As a result, there was some spreading of composition of the various species near interfaces, in addition to some actual interdiffusion between YSZ and GDC. Note however that the interdiffusion distance is no more than about 2 μm. The thickness of the YSZ layer was ~5 μm. Thus it is expected than in both locations of the YSZ layer, there was at least a couple microns of the YSZ layer with negligible amount of ceria dissolved in it.

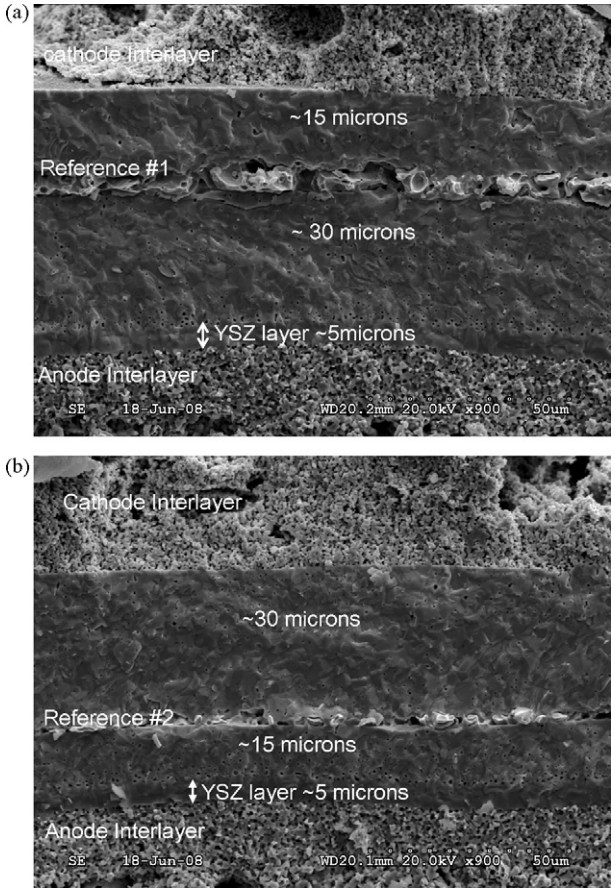

Fig. 2. SEM micrographs of the cross section of the cathode/GDC/YSZ/anode cell. (a) An SEM micrograph showing cathode interlayer (CF), GDC with embedded electrode Ref. #1, YSZ layer, and anode interlayer (AF). (b) An SEM micrograph showing cathode interlayer (CF), GDC with embedded electrode Ref. #2, YSZ, and anode interlayer (AF).

3.3. The measurement of ionic resistivities of GDC and YSZ in air

The resistivities of the GDC and YSZ bar-shaped samples at 650 °C in air were measured as ~19.5 Ω cm and ~58.8 Ω cm, respectively. Since GDC and YSZ are both predominantly oxygen ion conductors in air at 650 °C, the measured conductivities are attributed to oxygen ion conduction.

3.4. The measurement of reduced negative electrochemical potential of electrons, φ, or electric potential under open circuit, under load and under short circuit conditions

Fig. 5(a) and (b) shows the measured three voltages, $\Delta\varphi$, between the anode and Ref. #2, the anode and Ref. #1, and the anode and the cathode as a function of external load (short circuit to open circuit) in cathode/GDC/YSZ/anode and cathode/YSZ/GDC/anode bi-layer cells, respectively. The measured voltages with the embedded Pt electrodes correspond to the reduced negative electrochemical potential of electrons (or reduced electrochemical potential of holes), φ [22], in the electrolyte assuming that the sealing glass shuts down any oxygen exchange between the

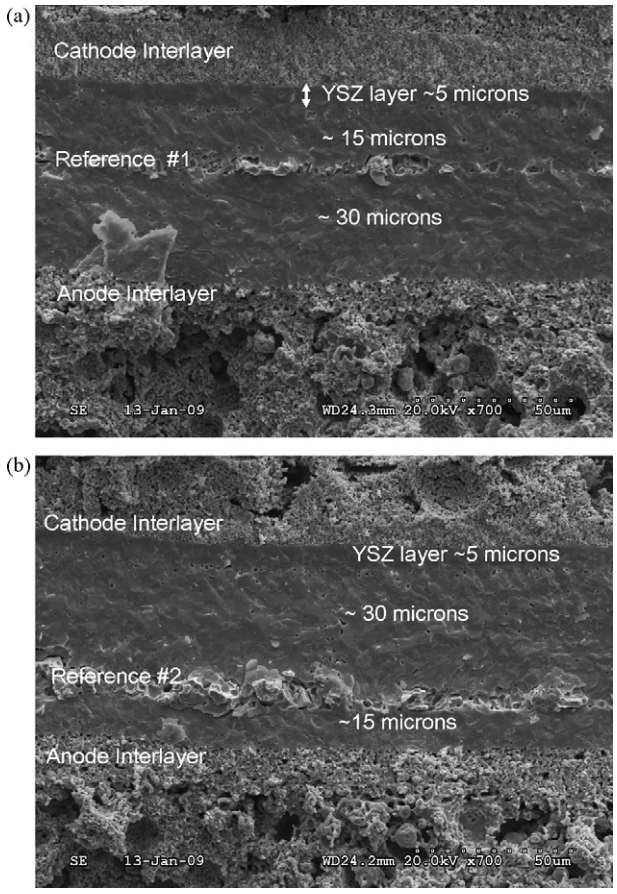

Fig. 3. SEM micrographs of the cross section of the cathode/YSZ/GDC/anode cell. (a) An SEM micrograph showing cathode interlayer (CF), YSZ, GDC with embedded electrode Ref. #1, and anode interlayer (AF). (b) An SEM micrograph showing cathode interlayer (CF), YSZ, GDC with embedded electrode Ref. #2, and anode interlayer (AF).

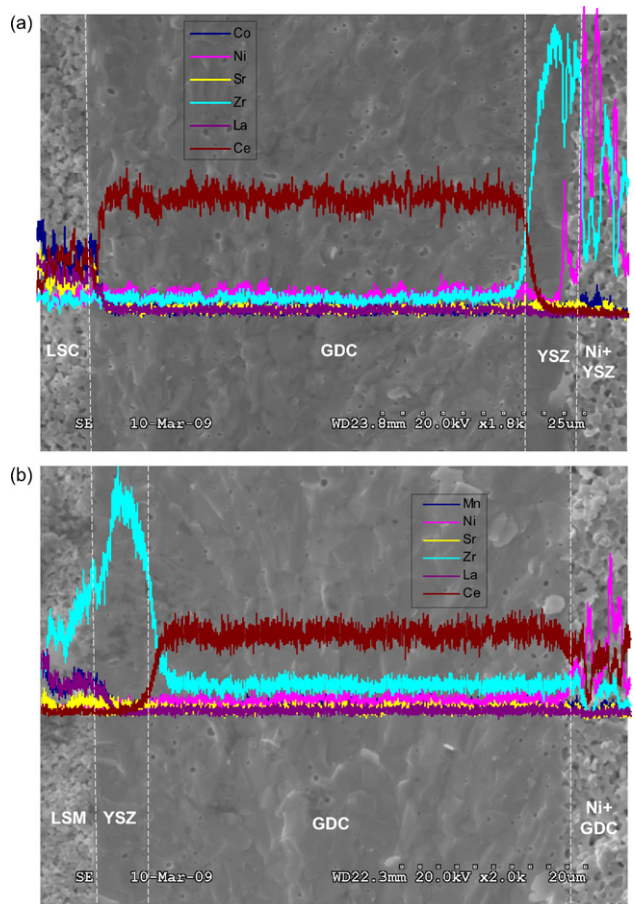

Fig. 4. EDAX scans across the bi-layer cells: (a) cathode/GDC/YSZ/anode cell and (b) cathode/YSZ/GDC/anode cell.

ambient atmosphere and the embedded electrodes[2] [21]. The measured φ was stable in both types of cells, cathode/GDC/YSZ/anode and cathode/YSZ/GDC/anode, which indicates that rapid local equilibration occurs (steady state established) and the embedded Pt probes readily exchange electrons with the GDC electrolyte. This is consistent with expectations since the open circuit voltage is lower than the corresponding Nernst voltage, in both bi-layer cells, indicating significant electronic conduction. Ideally, under all conditions (open circuit to short circuit), in *steady state* the φ within the electrolyte is bounded by the values at the cathode, φ^I, and the anode, φ^{II}. Fig. 5(a) shows this is the case for all situations except under the short circuit condition. Under short circuit condition, it is noted that the signs of $\varphi^I - \varphi^{\text{ref1}}$ and $\varphi^I - \varphi^{\text{ref2}}$ in the cathode/GDC/YSZ/anode cell are negative. Under short circuit condition, the electronic conduction through the electrolyte is negligible (ideally zero) and all electronic current flows through the external circuit. This means neutral oxygen permeation through the electrolyte (from cathode to anode) is also negligible (although the flux of O^{2-} ions obviously is maximum at short circuit). If the glass sealing is not perfect, some leakage of oxygen can occur through the glass seals to the probes (as discussed earlier). This effectively increases the local μ_{O_2}, which lowers the electron concentration (increases hole concentration), lowers μ_e (increases μ_h), and thus increases φ. The slightly higher values of φ^{ref1} and φ^{ref2} compared to φ^I thus indicate that the glass seal was good but not perfect. Fig. 5(b) shows that in the cathode/YSZ/GDC/anode cell under short circuit conditions, $\varphi^{\text{ref1}} - \varphi^{II}$ and $\varphi^{\text{ref2}} - \varphi^{II}$ are negative (with very small magnitudes). This is due either to experimental scatter or some transients.

In the case of the cathode/GDC/YSZ/anode cell, since YSZ is a predominantly ionic conductor even in a low p_{O_2} atmosphere, the YSZ layer between the anode interlayer and the GDC electrolyte essentially blocks off electronic leakage through the electrolyte. In such a case, the GDC is not reduced and should exhibit low electronic conduction. This effectively means lower μ_e in the GDC (than if the GDC had been exposed to hydrogen) and thus should lead to higher φ, compared to the cathode/YSZ/GDC/anode cell in which the GDC is partially reduced. Indeed, it is observed that in the cathode/GDC/YSZ/anode cell, the φ varies as a function of position; that is φ^{ref1} and φ^{ref2} are different with $\varphi^{\text{ref1}} > \varphi^{\text{ref2}}$ (except for short circuit condition as described above). By contrast, in the cathode/YSZ/GDC/anode cell, the GDC exposed to hydrogen is substantially reduced resulting in higher electron concentration, higher μ_e, higher electronic conduction, lower φ, and also effectively φ being independent of position. This result for the cathode/YSZ/GDC/anode cell compares with our earlier work on GDC-based single layer electrolyte cells and also with the results of Mineshighe et al. [20,21]. That is, in the case of the cathode/YSZ/GDC/anode cell, the voltage differences, $\Delta\varphi$, between the anode and the embedded reference electrodes in GDC are very small since the GDC is not protected from the reducing atmosphere, so that it is

[2] Actually even with the occurrence of oxygen leakage at embedded electrodes, the measured parameter is still φ. However, in such a case, the φ is influenced by oxygen leakage. Thus, to obtain a true measure of φ, the glass seal should prevent any oxygen leakage.

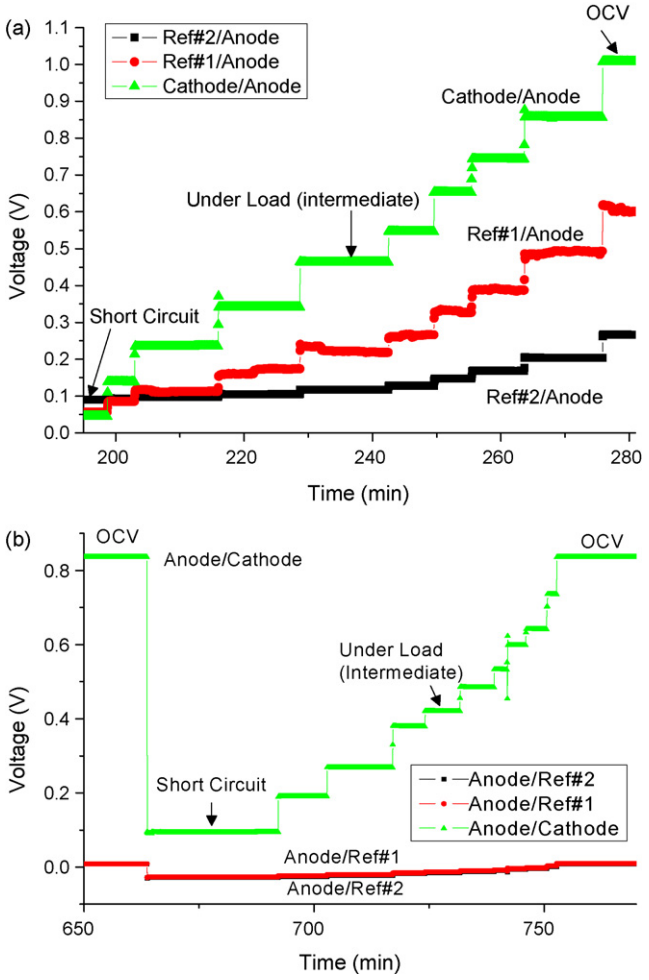

Fig. 5. (a) Measured voltages, $\Delta\varphi$, between the anode and Ref. #1, the anode and Ref. #2, and the anode and the cathode in the cathode/GDC/YSZ/anode cell at 650 °C with hydrogen/air under open circuit, under various loads, and under short circuit conditions. (b) Measured voltages, $\Delta\varphi$, between the anode and Ref. #1, the anode and Ref. #2, and the anode and the cathode in the cathode/YSZ/GDC/anode cell at 650 °C with hydrogen/air under open circuit, under various loads, and under short circuit conditions.

significantly reduced (higher electron concentration), which is similar to the φ measurement in GDC single layer electrolyte cell [21].

Based on the data given in Fig. 5(a) and (b), the φ through the cathode/GDC/YSZ/anode and the cathode/YSZ/GDC/anode cells are plotted in Fig. 6(a) and (b), respectively, under open circuit; in Fig. 6(c) and (d), respectively, under intermediate load; and in Fig. 6(e) and (f), respectively, under short circuit conditions. For simplicity, it was assumed that φ varies linearly as a function of position, which would be the case if the electronic conductivity of GDC is not a function of position. In general, the electronic conductivity is a function of μ_{O_2} (p_{O_2}) and thus is a function of position. Several probes will need to be embedded in order to determine the spatial (nonlinear) dependence of φ on position. The φ within the GDC layer of the cathode/GDC/YSZ/anode cell shows a monotonic variation while the φ within the GDC layer in the cathode/YSZ/GDC/anode cell is essentially flat and exhibits an abrupt change across the thin YSZ layer. As the cell operation mode was changed from short circuit to open circuit in the case of the cathode/GDC/YSZ/anode cell all three voltages between the anode and Ref. #1, the anode and Ref. #2 and the anode and the cathode correspondingly decreased. By contrast, in the case of the cathode/YSZ/GDC/anode cell, as the overall cell voltage decreases from open to short circuit, only the $\Delta\varphi$ across the thin YSZ layer at the cathode interface changes while $\varphi^{\text{ref1}} - \varphi^{\text{ref2}}$ and $\varphi^{\text{ref2}} - \varphi^{II}$ are essentially zero.

3.5. The cathode/GDC/YSZ/anode cell

In order to obtain an approximate estimate of the reduced negative electrochemical potential of electrons just inside the electrolyte at the cathode/electrolyte interface, φ^c, and just inside the GDC electrolyte at the GDC/YSZ interface, $\varphi^{(i)}$, in the cathode/GDC/YSZ/anode cell, the φ was assumed to be a linear function of position. Since Ref. #1 and Ref. #2 are symmetrically embedded in the GDC electrolyte, $\varphi^c - \varphi^{\text{ref1}}$, $\varphi^{\text{ref1}} - \varphi^{\text{ref2}}$ and $\varphi^{\text{ref2}} - \varphi^{(i)}$ should be about the same. Based on the assumption of linear dependence, at open circuit (Fig. 6(a)), the $\Delta\varphi$ across the cathode/electrolyte interface, $\varphi^{\text{I}} - \varphi^{\text{c}}$, is estimated as ~65 mV while that across the GDC/YSZ interface and anode, $\varphi^{(i)} - \varphi^{II}$, is negligible. Note that $\varphi^{\text{ref2}} - \varphi^{(i)}$ was set to be slightly different from $\varphi^{\text{ref1}} - \varphi^{\text{ref2}}$ and $\varphi^c - \varphi^{\text{ref1}}$. Since $\varphi^a - \varphi^{II} = r_e^a I_e \approx 0$, and since the steady state electronic current density, I_e, is not zero, it follows that the electronic resistance across the anode/electrolyte interface is negligible, that is, $r_e^a \approx 0$.

The electronic resistance across the cathode/electrolyte interface, r_e^c, and the electronic resistance of the bi-layer electrolyte, r_e^{el}, can be estimated as follows. At short circuit, I_e is ideally zero[3] so that the measured total current density, ~0.60 A cm^{-2}, is essentially all ionic. Thus, the ionic current density, I_i, at short circuit is given by $|-E/R_i| = 0.60\,\text{A cm}^{-2}$. The cell ionic area specific resistance, R_i, is thus estimated as $\sim 1.75\,\Omega\,\text{cm}^2$. The open circuit voltage, E_M, was measured as ~1.01 V, and the corresponding Nernst voltage, E, is ~1.05 V [21]. Using these values, the cell ionic transference number is given by $t_i \approx 1.01/1.05 = 0.962$.[4] Now, t_i is given by $t_i = R_e/(R_i + R_e) = E_M/E \approx 0.962$. Thus, the cell electronic area specific resistance, R_e is determined as $\sim 44.30\,\Omega\,\text{cm}^2$. From these values of ionic and electronic resistances, the leakage current at open circuit is estimated as $|I_i| = |I_e| = E/(R_i + R_e) \approx 0.023\,\text{A cm}^{-2}$. Therefore, the electronic area specific resistance across the cathode/electrolyte interface is given by $r_e^c = (\varphi^I - \varphi^c)/|I_e| = (0.065/0.023)\,\Omega\,\text{cm}^2$, that is $\sim 2.82\,\Omega\,\text{cm}^2$. Subtracting $r_e^c \approx 2.82\,\Omega\,\text{cm}^2$ from $R_e \approx 44.30\,\Omega\,\text{cm}^2$, the electronic area specific resistance across the bulk GDC/YSZ bi-layer, r_e^{el}, is determined as $\sim 41.48\,\Omega\,\text{cm}^2$.

Prior work by Mineshige et al. showed that in an RDC exposed to a reducing atmosphere, the μ_{O_2} equilibrated across the gas/solid interface [20]. Experiments conducted by the present authors also showed that the μ_{O_2} equilibrated across the electrolyte/anode interface with a GDC electrolyte [21]. In addition, the measurement of φ showed that it also equilibrated across the electrolyte/anode interface. These observations are consistent with $r_e^a \approx 0$ and $r_i^a \approx 0$. It is assumed here that in the present case of cathode/GDC/YSZ/anode cell also $r_i^a \approx 0$.

The average ionic conductivity of bulk GDC/YSZ bi-layer, $\sigma_i^{\text{GDC/YSZ}}$, can be estimated as follows. In steady state, the divergences of ionic and electronic currents are separately zero; which means the ionic and the electronic currents are spatially invariant. In such a case, the ionic current is the same through both GDC and YSZ layers and is given by $|I_i| = \sigma_i^{\text{GDC}}(\tilde{\mu}^c_{O^{2-}} - \tilde{\mu}^{(i)}_{O^{2-}})/(2e\ell_{\text{GDC}}) = \sigma_i^{\text{YSZ}}(\tilde{\mu}^{(i)}_{O^{2-}} - \tilde{\mu}^a_{O^{2-}})/(2e\ell_{\text{YSZ}})$ where ℓ_{GDC} and ℓ_{YSZ} are respectively the thicknesses of the GDC and YSZ layers, and $\tilde{\mu}^{(i)}_{O^{2-}}$ is the electrochemical potential of

[3] In the experiment it was not exactly zero since the external short was not an ideal short—it had some nonzero resistance.

[4] This is for the cell including electrolyte/electrode interfaces, and not only for the electrolyte, as discussed in [23].

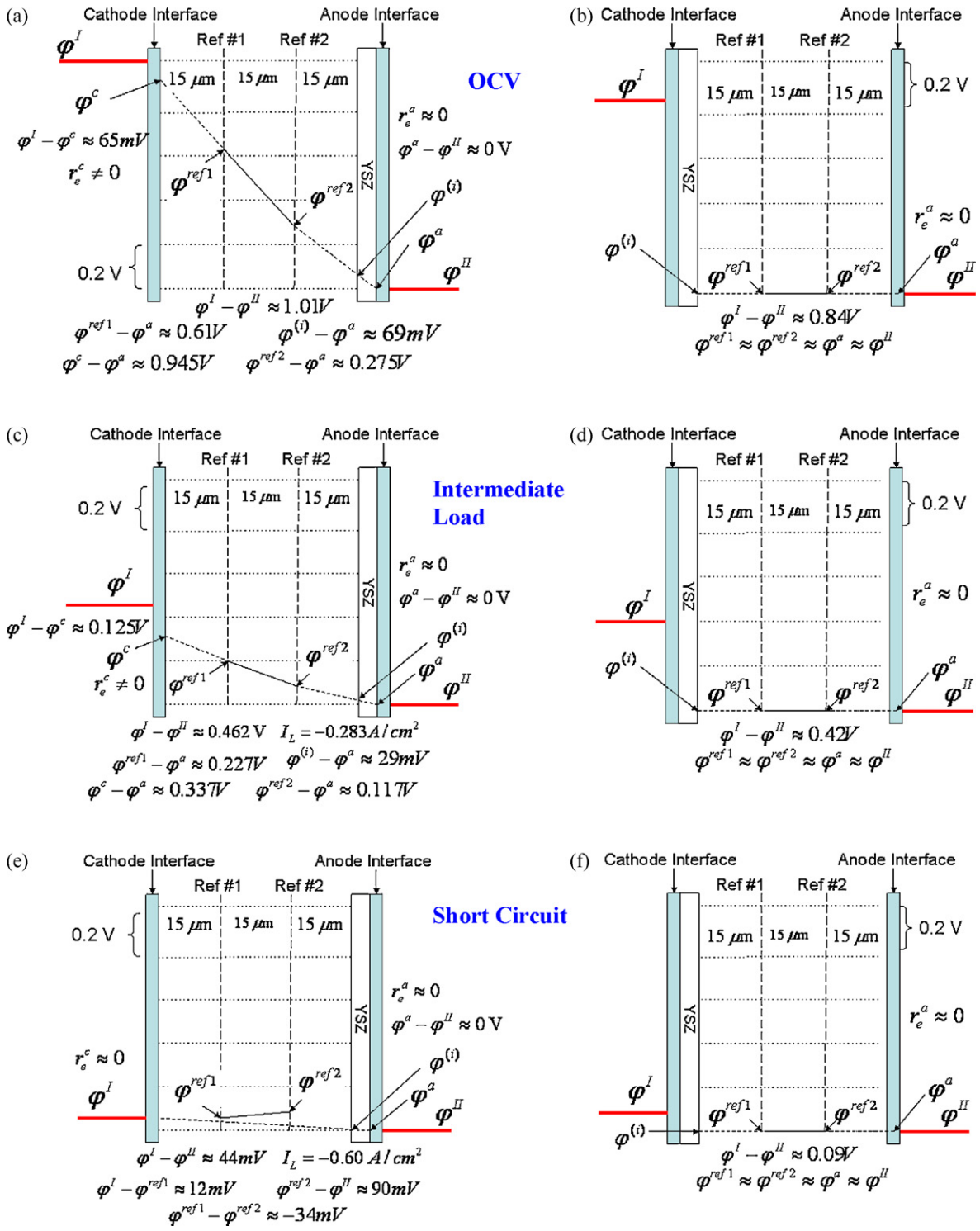

Fig. 6. Plots of the measured φ in the cathode/GDC/YSZ/anode cell under open circuit (a), under intermediate load (c), and under short circuit condition (e). Plots of the measured φ in the cathode/YSZ/GDC/anode cell under open circuit (b), under intermediate load (d), and under short circuit condition (f).

oxygen ions at the interface between GDC and YSZ layers.[5] Under OCV conditions, this is given by $|I_i| = |I_e| = 0.023\ \mathrm{A\,cm^{-2}}$. Since we know the σ_i^{GDC} and σ_i^{YSZ}, the corresponding $(\tilde{\mu}^c_{O^{2-}} - \tilde{\mu}^{(i)}_{O^{2-}})/(2e)$ and $(\tilde{\mu}^{(i)}_{O^{2-}} - \tilde{\mu}^a_{O^{2-}})/(2e)$ are estimated as $\sim 2.07 \times 10^{-3}$ V and $\sim 6.76 \times 10^{-4}$ V, respectively. Thus, the net change in $\tilde{\mu}_{O^{2-}}/(2e)$ at OCV across the entire bi-layer is determined as $(\tilde{\mu}^c_{O^{2-}} - \tilde{\mu}^a_{O^{2-}})/(2e) = (\tilde{\mu}^c_{O^{2-}} - \tilde{\mu}^{(i)}_{O^{2-}})/(2e) + (\tilde{\mu}^{(i)}_{O^{2-}} - \tilde{\mu}^a_{O^{2-}})/(2e) \approx 2.756 \times 10^{-3}$ V. Using this value and the steady state leakage current, $|I_i|$, the average $\sigma_i^{GDC/YSZ}$ is estimated as $\sim 0.042\ \mathrm{S\,cm^{-1}}$. Thus, the area specific ionic resistance across the bulk bi-layer is estimated as $r_i^{el} \approx (50 \times 10^{-4}/0.042) \approx 0.12\ \Omega\,\mathrm{cm^2}$. Now, subtracting r_i^{el} from R_i and noting that $r_i^a \approx 0$, the r_i^c is estimated as $\sim 1.63\ \Omega\,\mathrm{cm^2}$.

[5] This assumes that there is negligible change in $\tilde{\mu}_{O^{2-}}$ across the GDC/YSZ or YSZ/GDC interface.

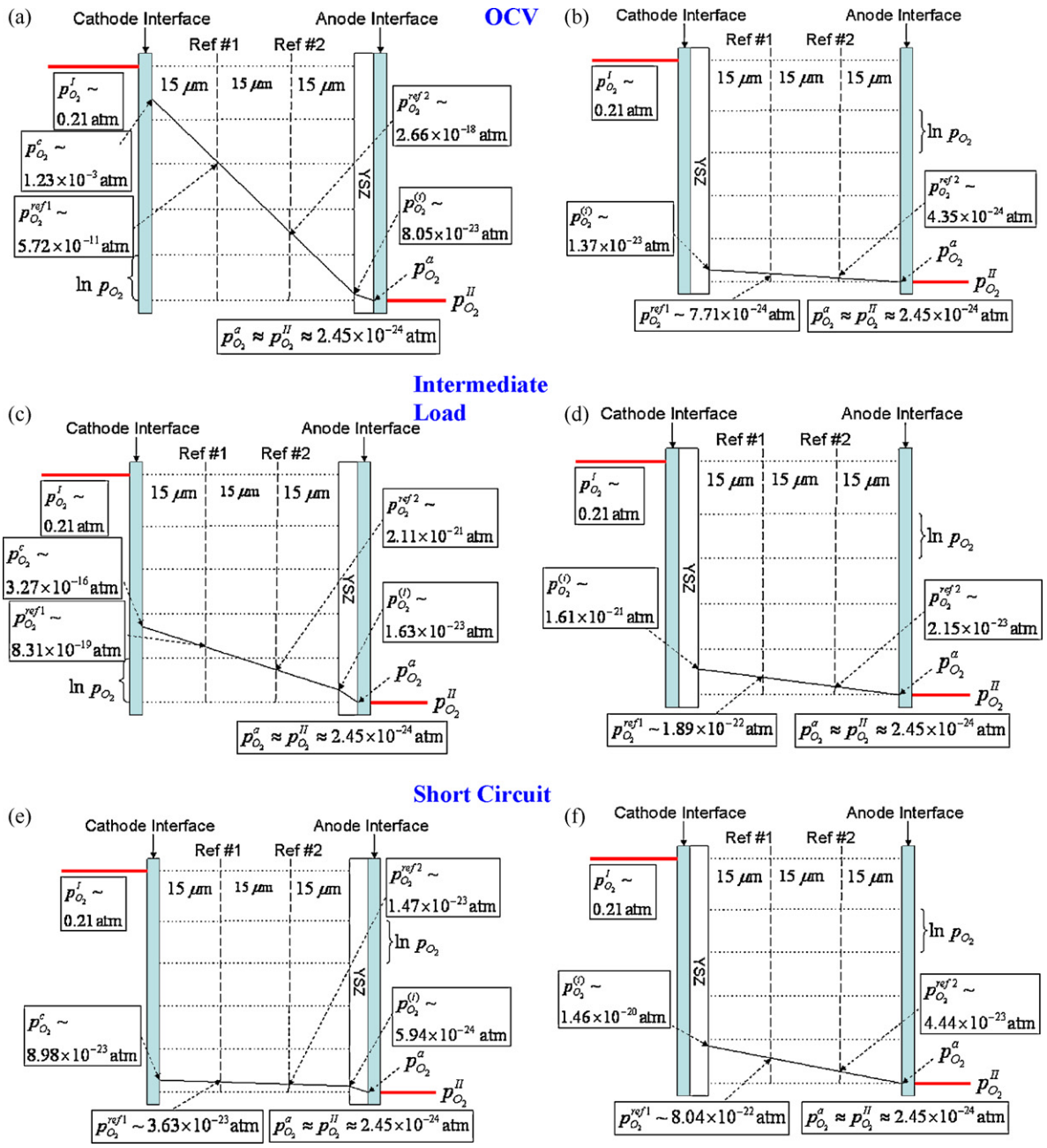

Fig. 7. Plots of the estimated p_{O_2} in the cathode/GDC/YSZ/anode cell under open circuit (a), under intermediate load (c), and under short circuit condition (e). Plots of the estimated p_{O_2} in the cathode/YSZ/GDC/anode cell under open circuit (b), under intermediate load (d) and under short circuit condition (f).

This is a measure of the cathode polarization resistance (excluding contribution from the extended porous cathode).

Similarly, it is assumed that $\varphi^{c} - \varphi^{\text{ref1}} \approx \varphi^{\text{ref1}} - \varphi^{\text{ref2}} \approx \varphi^{\text{ref2}} - \varphi^{a}$ (note that $\varphi^{(i)} \sim \varphi^{a}$) under all load conditions. At an intermediate load (corresponding to load current, $I_L = -0.283\,\text{A cm}^{-2}$), the $\Delta\varphi = \varphi^{I} - \varphi^{c}$ across the cathode/electrolyte interface for the cathode/GDC/YSZ/anode cell is estimated as ~125 mV, while that across the anode/electrolyte interface is negligible. Ideally, it would be expected that $\Delta\varphi = \varphi^{I} - \varphi^{c}$ would be lower under load than that under OCV (~65 mV). A higher value of the $\Delta\varphi$ under load is not expected and the reason for this observation is not known. Perhaps this is related to the approximation made concerning linear variation of φ which is strictly not accurate. Also, φ^{ref1} and φ^{ref2} are not accurate due to some oxygen leakage at the probes. At short circuit, the overall cell voltage, $\varphi^{I} - \varphi^{II}$, was measured as ~44 mV. Ideally, the φ^{ref1} and φ^{ref2} must be bounded by the values at the electrodes, φ^{I} and φ^{II} [23,24]. The observation that they are not bounded, that is the measured $\varphi^{\text{ref2}} - \varphi^{II}$ is slightly larger than $\varphi^{I} - \varphi^{II}$, is attributed to some oxygen leakage into the GDC through the glass seal as discussed earlier.

3.6. The cathode/YSZ/GDC/anode cell

In the cathode/YSZ/GDC/anode cell, the OCV was ~0.84 V. The corresponding cell transference number is $t_i = E_M/E = 0.84/1.05 = 0.8 = R_e/(R_i/R_e)$. Also, the measured short circuit current density was $2.0\,\text{A cm}^{-2}$, or $|-E/R_i| = 2.0\,\text{A cm}^{-2}$. From these measurements, the estimated values of the cell ionic and electronic area specific resistances are $R_i = 0.525\,\Omega\,\text{cm}^2$ and $R_e = 2.1\,\Omega\,\text{cm}^2$. Also, the leakage current density at OCV is

$|I_i| = |I_e| = E/(R_i + R_e) = 0.4\,\mathrm{A\,cm^{-2}}$, which is rather high and suggests that in this cell substantial electronic leakage occurs through the YSZ layer.

In the cathode/YSZ/GDC/anode cell, the φ was essentially constant throughout the GDC layer regardless of the load, and was about the same as φ^a; that is, $\varphi^{GDC} - \varphi^a \approx 0$. Most of the $\Delta\varphi$ thus dropped across the cathode/YSZ/GDC region, across the YSZ layer. No Pt probes were embedded in the YSZ layer in either of the cells. Thus, the variation of φ through the YSZ layer could not be estimated. However, it is clear that the $\Delta\varphi$ through the YSZ layer must be large due to its higher electronic resistance compared to GDC so that $\Delta\varphi$ across the cathode/electrolyte interface, $\varphi^I - \varphi^c$, probably is not large, similar to the cathode/GDC/YSZ/anode cell. The estimated electronic resistance of the cell is $R_e \approx 2.1\,\Omega\,\mathrm{cm^2}$ and the leakage current at OCV is $\sim 0.4\,\mathrm{A\,cm^{-2}}$. Much of the electronic resistance is associated with the YSZ layer and cathode/YSZ interface. Thus, the $\Delta\varphi = \varphi^I - \varphi^{(i)} \approx 0.4 \times 2.1 = 0.84\,\mathrm{V}$, that is most of the OCV. Also, note that due to the partial reduction of GDC in the cathode/YSZ/GDC/anode cell leading to the creation of significant electronic conduction in GDC, only the YSZ layer and probably a very thin unreduced GDC layer functions as the effective electrolyte. This is in contrast to the cathode/GDC/YSZ/anode cell in which the GDC is not reduced, is a predominantly oxygen ion conductor, and the entire GDC/YSZ layer functions as the electrolyte.

3.7. The estimation of oxygen partial pressure, p_{O_2}, in GDC using the measurements of φ under OCV, under load and under short circuit conditions

The partial pressure of oxygen, p_{O_2}, within the GDC layer can be estimated using the relation between $\tilde{\mu}_{O^{2-}}$ and μ_{O_2} based on the assumption of local equilibrium given by [21,23]

$$p_{O_2}(x) = p^a_{O_2}\ \exp\left[\frac{4e(\varphi(x) - \varphi^a) + 2(\tilde{\mu}_{O^{2-}}(x) - \tilde{\mu}^a_{O^{2-}})}{k_B T}\right] \tag{3}$$

where x is distance from the anode/electrolyte interface, and all parameters with superscript a correspond to values within the electrolyte, just inside the anode/electrolyte interface. Since $r^a_i \approx 0$ and $r^a_e \approx 0$, we have $\varphi^a \approx \varphi^{II}$, $\mu^a_{O_2} \approx \mu^{II}_{O_2}$, $p^a_{O_2} \approx p^{II}_{O_2}$, and $\tilde{\mu}^a_{O^{2-}} \approx \tilde{\mu}^{II}_{O^{2-}}$.

For the cathode/GDC/YSZ/anode cell, since we already have the values of $\varphi^c - \varphi^a$ and $(\tilde{\mu}^c_{O^{2-}} - \tilde{\mu}^a_{O^{2-}})/(2e)$, the $p^c_{O_2}$ can be readily estimated. At OCV, the $p^c_{O_2}$ is estimated as $\sim 1.23 \times 10^{-3}$ atm (Fig. 7(a)). The oxygen pressure in the gas phase at the cathode is $p^I_{O_2} \sim 0.21$ atm. Thus, the change in $\ln p_{O_2}$ across the cathode/electrolyte interface, $\Delta \ln p_{O_2} = \ln 0.21 - \ln(1.23 \times 10^{-3})$, is rather small. By comparison, in the cell made with a GDC single layer electrolyte of an earlier study, the estimated $p^c_{O_2}$ was $\sim 2.0 \times 10^{-21}$ atm, with a correspondingly large $\Delta \ln p_{O_2}$ [21]. The higher $p^c_{O_2}$ in the cathode/GDC/YSZ/anode bi-layer electrolyte cell of the present study is attributed to the YSZ protecting layer positioned at the anode side. The YSZ layer suppresses electronic conduction through the GDC electrolyte so that the GDC is a predominantly ionic conductor in the cathode/GDC/YSZ/anode bi-layer electrolyte cell. By contrast, $\Delta \ln p_{O_2}$ across the cathode/electrolyte interface is large in a single GDC layer cell since then GDC is a mixed ionic and electronic conductor (MIEC) with significant electronic conduction [21]. This means in a GDC single layer electrolyte, much of the $\Delta\mu_{O_2}$ drops across the cathode/electrolyte interface [21].

In terms of the ionic current density through the electrolyte, I_i, and distance, x, measured into the electrolyte from the anode/electrolyte interface, Eq. (3) can be given as

$$p_{O_2}(x) = p^a_{O_2}\ \exp\left[\frac{4e(\varphi(x) - \varphi^a)}{k_B T} + \frac{2e|I_i|x}{\sigma_{O^{2-}} k_B T}\right] \tag{4}$$

In the cathode/GDC/YSZ/anode cell, the $\varphi(x) - \varphi^a \geq 0$. From the measured $\varphi^{ref1} - \varphi^a$, $\varphi^{ref2} - \varphi^a$, the assumption of linear dependence of $\varphi(x)$ on x, and the estimated ionic current density, I_i (corresponding to the measured load current), the oxygen partial pressure, $p_{O_2}(x)$, was estimated. At OCV, the leakage current is estimated as $|I_i| \sim 0.023\,\mathrm{A\,cm^{-2}}$. The estimated oxygen partial pressures at the two reference electrodes and at the GDC/YSZ interface are, respectively, $p^{ref1}_{O_2} \sim 5.72 \times 10^{-11}$ atm, $p^{ref2}_{O_2} \sim 2.66 \times 10^{-18}$ atm, and $p^{(i)}_{O_2} \sim 8.05 \times 10^{-23}$ atm. Using Eq. (4), oxygen partial pressures within the GDC layer corresponding intermediate load and short circuit conditions were similarly estimated. Fig. 7(c) shows the various p_{O_2}'s for the intermediate load. They are, $p^c_{O_2} \sim 3.27 \times 10^{-16}$ atm, $p^{ref1}_{O_2} \sim 8.31 \times 10^{-19}$ atm, $p^{ref2}_{O_2} \sim 2.11 \times 10^{-21}$ atm, and $p^{(i)}_{O_2} \sim 1.63 \times 10^{-23}$ atm. Fig. 7(e) shows the various p_{O_2}'s corresponding to the short circuit condition. They are $p^c_{O_2} \sim 8.98 \times 10^{-23}$ atm, $p^{ref1}_{O_2} \sim 3.63 \times 10^{-23}$ atm, $p^{ref2}_{O_2} \sim 1.47 \times 10^{-23}$ atm, and $p^{(i)}_{O_2} \sim 5.94 \times 10^{-24}$ atm. These results shows that as the load is varied between OCV and short circuit, the p_{O_2} within the GDC electrolyte layer decreases. An examination of Eq. (4) shows that there are two terms in the exponent; one containing $\varphi(x) - \varphi^a$ and the other containing $|I_i|$. As the load is varied between OCV and short circuit, the $|I_i|$ increases but $\varphi(x) - \varphi^a$ decreases. The net effect is to lower the $p_{O_2}(x)$.

Now, let us examine the cathode/YSZ/GDC/anode cell. In the cathode/YSZ/GDC/anode cell, throughout the GDC electrolyte, we have $\varphi(x) - \varphi^a \approx 0$ over all conditions (OCV, under load, and short circuit) due to its very high electronic conductivity. Thus, the $p_{O_2}(x)$ is approximately given by

$$p_{O_2}(x) \approx p^a_{O_2}\ \exp\left[\frac{2e|I_i|x}{\sigma_{O^{2-}} k_B T}\right] \tag{5}$$

Thus, in this case the only term in the exponent is that containing $|I_i|$. Note that at OCV, the $|I_i|$ has its lowest magnitude. As the load increases from OCV to intermediate to short circuit, the $|I_i|$ increases. Thus, we expect that in this case the oxygen pressure within the GDC to increase with increasing current. Indeed, experimental measurements are in accord with this expectation. Fig. 7(b) shows the various p_{O_2}'s corresponding to the OCV. They are, $p^{(i)}_{O_2} \sim 1.37 \times 10^{-23}$ atm, $p^{ref1}_{O_2} \sim 7.71 \times 10^{-24}$ atm, and $p^{ref2}_{O_2} \sim 4.35 \times 10^{-24}$ atm. Fig. 7(d) shows the various p_{O_2}'s corresponding to the intermediate load. They are, $p^{(i)}_{O_2} \sim 1.61 \times 10^{-21}$ atm, $p^{ref1}_{O_2} \sim 1.89 \times 10^{-22}$ atm, and $p^{ref2}_{O_2} \sim 2.15 \times 10^{-23}$ atm. Finally, Fig. 7(f) shows the various p_{O_2}'s corresponding to the short circuit condition. They are, $p^{(i)}_{O_2} \sim 1.46 \times 10^{-20}$ atm, $p^{ref1}_{O_2} \sim 8.04 \times 10^{-22}$ atm, and $p^{ref2}_{O_2} \sim 4.44 \times 10^{-23}$ atm. These results show that as the load current increases, in this case, the $p_{O_2}(x)$ within the GDC layer increases.

The above-described results concerning the variation of $p_{O_2}(x)$ as a function of load current in bi-layer electrolyte fuel cells are in accord with prior theoretical work by Virkar [4] and Marques and Navarro [5,6]. Virkar examined interface $p^{(i)}_{O_2}$ as a function of load condition for two types of bi-layer cells; one with cathode side layer having higher electronic conductivity (e.g. GDC) than the anode-side layer (e.g. YSZ) and the other with cathode-side layer having lower electronic conductivity (e.g. YSZ) than the anode-side layer (e.g. GDC) [4]. In the former case, the $p^{(i)}_{O_2}$ decreased with increasing load current while in the latter case the $p^{(i)}_{O_2}$ increased with increasing load current, in accord with the present experimental results. Marques et al. also examined a bi-layer cell and numerically estimated the $p^{(i)}_{O_2}$ as a function of

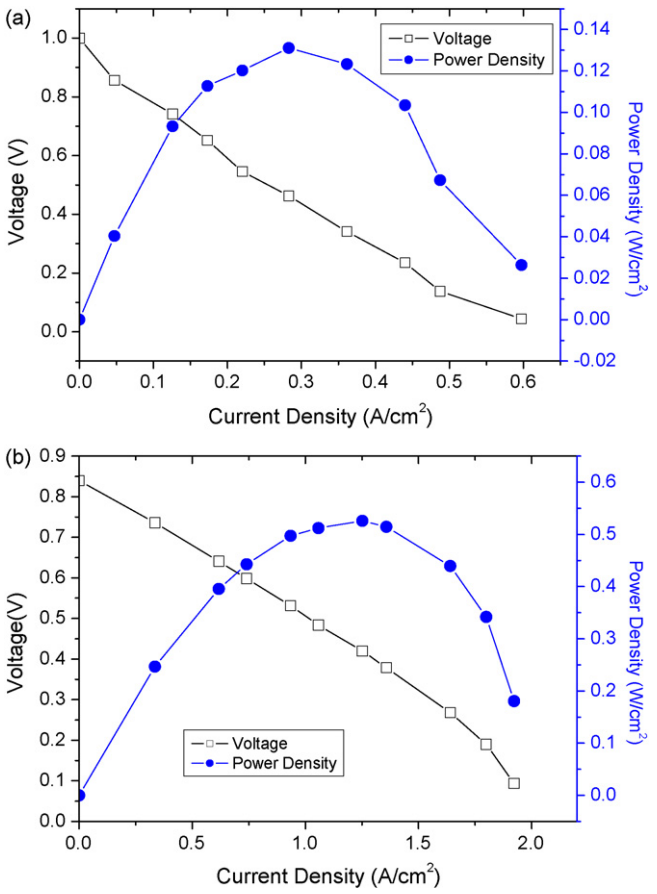

Fig. 8. (a) Voltage and power density vs. current density performance curves for the cathode/GDC/YSZ/anode cell at 650 °C under hydrogen/air. (b) Voltage and power density vs. current density performance curves for the cathode/YSZ/GDC/anode cell at 650 °C under hydrogen/air.

the relative location of the YSZ layer and the results were similar [5,6].

3.8. The performance of cathode/GDC/YSZ/anode and cathode/YSZ/GDC/anode cells

Fig. 8(a) and (b) shows voltage vs. current density and power density vs. current density plots at 650 °C for the cathode/GDC/YSZ/anode cell and the cathode/YSZ/GDC/anode cell, respectively. The maximum power density for the cathode/GDC/YSZ/anode cell was ~0.14 W cm^{-2}. By contrast, the maximum power density for the cathode/YSZ/GDC/anode cell was ~0.52 W cm^{-2}, or greater by more than a factor of three. This high power density of the cathode/YSZ/GDC/anode cell was despite the fact that: (i) the bi-layer electrolyte thickness was the same in both cells, (ii) the OCV was lower in the cathode/YSZ/GDC/anode cell, and (iii) this cell also had LSM + YSZ cathode, which is generally considered to be less active than LSC + GDC cathode. An analysis of this higher performance in the cathode/YSZ/GDC/anode cell is presented in what follows.

Fig. 9(a) and (b) is simplified equivalent circuit for the two types of cells. Concentration polarization and that part of the activation polarization associated with extended porous electrodes are ignored in the following discussion. However, activation polarizations attributed to the physically sharp electrolyte/electrode interfaces are included. These are described by r_i^c and r_i^a. The net ionic and electronic area specific resistances of the cells are given by

$$R_i' = r_i^{c'} + r_i^{\mathrm{GDC}'} + r_i^{\mathrm{YSZ}'} + r_i^{a'} \tag{6a}$$

$$R_i'' = r_i^{c''} + r_i^{\mathrm{YSZ}''} + r_i^{\mathrm{GDC}''} + r_i^{a''} \tag{6b}$$

$$R_e' = r_e^{c'} + r_e^{\mathrm{GDC}'} + r_e^{\mathrm{YSZ}'} + r_e^{a'} \tag{6c}$$

$$R_e'' = r_e^{c''} + r_e^{\mathrm{YSZ}''} + r_e^{\mathrm{GDC}''} + r_e^{a''} \tag{6d}$$

In general, the ionic and the electronic resistances for the two different bi-layer configurations may be different. For this reason, primes and double primes are used in the notations. From OCV and short circuit current density measurements, we have estimates of the ionic area specific resistances for the two cells. They are $R_i' \approx 1.75\,\Omega\,\mathrm{cm}^2$ and $R_i'' \approx 0.525\,\Omega\,\mathrm{cm}^2$. In both cells, equilibration of μ_{O_2} across the electrolyte/anode interfaces gives, $r_i^{a'} \approx 0$ and $r_i^{a''} \approx 0$. Also, as the ionic conductivities of YSZ and GDC are essentially independent of oxygen pressure (extrinsically controlled by the dopants), we have $r_i^{\mathrm{YSZ}'} = r_i^{\mathrm{YSZ}''} = r_i^{\mathrm{YSZ}}$ and $r_i^{\mathrm{GDC}'} = r_i^{\mathrm{GDC}''} = r_i^{\mathrm{GDC}}$. Thus, $r_i^{\mathrm{YSZ}'} + r_i^{\mathrm{GDC}'} = r_i^{\mathrm{YSZ}''} + r_i^{\mathrm{GDC}''} = r_i^{\mathrm{el}}$. But we know from the conductivity measurements of the GDC and YSZ samples and the bi-layer electrolyte thickness that $r_i^{\mathrm{el}} \approx 0.12\,\Omega\,\mathrm{cm}^2$. Thus, the R_i' and R_i'' simplify to

$$R_i' = r_i^{c'} + r_i^{\mathrm{GDC}'} + r_i^{\mathrm{YSZ}'} + r_i^{a'} \approx r_i^{c'} + r_i^{\mathrm{el}} \approx r_i^{c'} + 0.12 = 1.75\,\Omega\,\mathrm{cm}^2 \tag{7a}$$

and

$$R_i'' = r_i^{c''} + r_i^{\mathrm{YSZ}''} + r_i^{\mathrm{GDC}''} + r_i^{a''} \approx r_i^{c''} + r_i^{\mathrm{el}} \approx r_i^{c''} + 0.12 = 0.525\,\Omega\,\mathrm{cm}^2 \tag{7b}$$

From the above, the estimated values of cathode/electrolyte ion transfer resistances for the cathode/GDC/YSZ/anode and the cathode/YSZ/GDC/anode cells are estimated respectively as $r_i^{c'} \approx 1.63\,\Omega\,\mathrm{cm}^2$ and $r_i^{c''} \approx 0.405\,\Omega\,\mathrm{cm}^2$. This is quite a remarkable result in that it shows that the location of the YSZ layer (either at the cathode side or the anode side) substantially influences the cathode activation polarization resistance. While independent measurements will be required to confirm these findings, it is useful to seek a possible explanation of this behavior. In the cathode/GDC/YSZ/anode cell, the drop in oxygen chemical potential across the cathode/electrolyte interface is modest; it is given by (at OCV)

$$\Delta\mu_{O_2} = \mu_{O_2}^I - \mu_{O_2}^c = k_B T \ln\left(\frac{0.21}{1.23\times10^{-3}}\right) = 5.14 k_B T = 4.744\times10^3 k_B \tag{8a}$$

In the cathode/YSZ/GDC/anode cell, the magnitude of oxygen chemical potential drop across the cathode/electrolyte interface could not be determined as no reference electrode was embedded in the YSZ layer. However, the chemical potential drop across the YSZ layer can be estimated. At OCV, it is given by

$$\Delta\mu_{O_2} = \mu_{O_2}^I - \mu_{O_2}^{(i)} = k_B T \ln\left(\frac{0.21}{1.37\times10^{-23}}\right) = 51.08 k_B T = 4.715\times10^4 k_B \tag{8b}$$

This is ten times the drop in μ_{O_2} in the cathode/GDC/YSZ/anode cell. It may be reasonably assumed that the overall process of oxygen incorporation across the cathode/electrolyte interface will be aided by the chemical potential change—the larger the $\Delta\mu_{O_2}$, the lower should be the activation polarization resistance. The

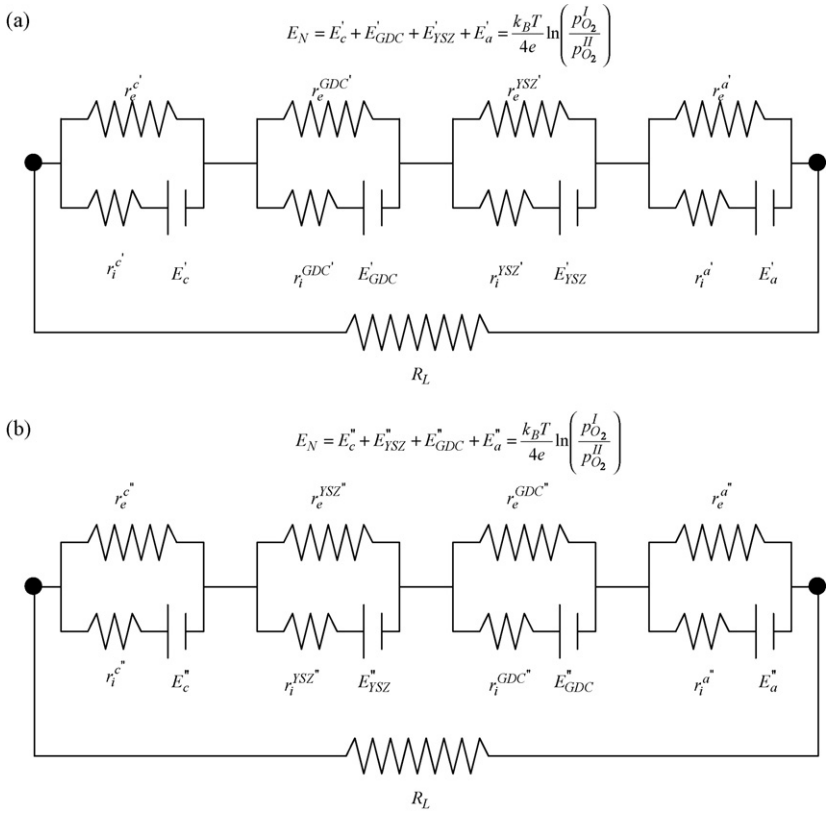

Fig. 9. (a) A simplified equivalent circuit for the cathode/GDC/YSZ/anode cell. (b) A simplified equivalent circuit for the cathode/YSZ/GDC/anode cell.

lower activation polarization resistance at the cathode for the cathode/YSZ/GDC/anode cell is thus attributed to the large drop in μ_{O_2} across the interface. The cathode/YSZ/GDC/anode cell had a lower OCV. The cathode of this cell was fired at a somewhat higher temperature (~1170 °C) compared to the cathode/GDC/YSZ/anode cell. Perhaps some diffusion of Mn may have occurred into the thin YSZ layer increasing its electronic conductivity. Indeed, prior work on LSM cathodes on YSZ has shown that depending upon the firing conditions, Mn can diffuse into YSZ forming a layer with higher electronic conductivity than baseline YSZ [25]. Fig. 4(b) also shows that there may have been some diffusion of Mn into the YSZ layer. It would appear that suitable changes can be made in processing such that the OCV can be increased for the cathode/YSZ/GDC/anode cell. If this is achieved, even higher performance may be possible. The present results thus show that the location of the YSZ layer determines the overall cathode activation polarization and the cell performance, and that the preferred location of the YSZ thin layer in YSZ–GDC bi-layer electrolyte anode-supported cells is between the cathode and the GDC electrolyte.

4. Summary

Anode-supported cells with GDC/YSZ (YSZ/GDC) bi-layer electrolyte of thickness ~45 μm GDC and ~5 μm YSZ, LSC + GDC (LSM + YSZ) cathode interlayer, Ni + YSZ (Ni + GDC) anode interlayer, and Ni + YSZ anode support were fabricated with two Pt probes embedded within the GDC layer. A glass was used to seal off the embedded probes from the atmosphere. The reduced negative electrochemical potential of electrons (electric potential), φ, through the GDC electrolyte as a function of position was measured at 650 °C using the embedded probes, with air circulated past the cathode and hydrogen past the anode, under open circuit, under various loads, and under short circuit. It was observed that the φ in the GDC layer of the cathode/GDC/YSZ/anode cell was a function of load and varied as a function of position. By contrast, the φ in the GDC layer of the cathode/YSZ/GDC/anode cell was nearly independent of position (and load) and was about the same as that at the anode, φ^{II}. From these measurements and the measurement of performance curves (voltage vs. current density), the oxygen partial pressure (chemical potential), p_{O_2} (μ_{O_2}), within the GDC electrolyte was estimated as a function of position at various load conditions (open circuit, under load, and short circuit). The most striking difference between the two cells was that in the cathode/YSZ/GDC/anode cell, there was a sharp change in ln p_{O_2} across the cathode/YSZ region. By contrast, there was a relatively small change in ln p_{O_2} across the cathode/GDC interface in the cathode/GDC/YSZ/anode cell. It was also observed that the cathode/YSZ/GDC/anode cell exhibited over three times the performance of the cathode/GDC/YSZ/anode cell, despite the same total electrolyte thickness. This vast difference in performance depending upon the location of the YSZ layer was attributed to a large difference in the cathode/electrolyte ionic charge transfer resistance, r_i^c, which is essentially the cathode polarization resistance. That is, the cathode/YSZ/GDC/anode cell exhibited much lower cathode polarization compared to the cathode/GDC/YSZ/anode cell. This is despite the fact that the cathode/GDC/YSZ/anode cell had LSC + GDC cathode functional layer, which is generally considered superior to LSM + YSZ, the latter being the cathode functional layer of the higher performing cathode/YSZ/GDC/anode cell. The present results thus suggest that in ceria-based anode-supported cells with a YSZ electron blocking layer, the location of the YSZ layer does determine the cell performance. The preferred location of the YSZ layer is between the cathode and the GDC electrolyte.

Acknowledgement

This work was funded by the U.S. Department of Energy under Grant Number DE-FG02-06ER46086.

References

[1] H. Yashiro, Y. Baba, K. Eguchi, H. Arai, J. Electrochem. Soc. 135 (1988) 2077.
[2] T. Inoue, T. Setoguchi, K. Eguchi, H. Arai, Solid State Ionics 35 (1989) 285.
[3] K. Eguchi, T. Setoguchi, T. Inoue, H. Arai, Solid State Ionics 52 (1992) 165.
[4] A.V. Virkar, J. Electrochem. Soc. 138 (1991) 1481.
[5] F.M.B. Marques, L.M. Navarro, Solid State Ionics 90 (1996) 183.
[6] F.M.B. Marques, L.M. Navarro, Solid State Ionics 100 (1997) 29.
[7] S.H. Chan, X.J. Chen, K.A. Khor, Solid State Ionics 158 (2003) 29.
[8] Q.L. Liu, K.A. Khor, S.H. Chan, X.J. Chen, J. Power Sources 162 (2006) 1036.
[9] C. Brahim, A. Ringuede, E. Gourba, M. Cassir, A. Billard, P. Briois, J. Power Sources 156 (2006) 45.
[10] D. Yang, X. Zhang, S. Nikumb, C. Deces-Petit, R. Hui, R. Maric, D. Ghosh, J. Power Sources 164 (2007) 182.
[11] M. Matsuda, T. Hosomi, K. Murata, T. Fukui, M. Miyake, J. Power Sources 165 (2007) 102.
[12] X. Zhang, M. Robertson, C. Deces-Petit, Y. Xie, R. Hui, W. Qu, O. Kesler, R. Maric, D. Ghosh, J. Power Sources 175 (2008) 800.
[13] P. Soral, U. Pal, W.L. Worrell, J. Electrochem. Soc. 145 (1998) 99.
[14] S. Yuan, U. Pal, P. Soral, J. Electrochem. Soc. 143 (1996) 3214.
[15] N.S. Choudhury, J.W. Patterson, J. Electrochem. Soc. 117 (1970) 1384.
[16] N.S. Choudhury, J.W. Patterson, J. Electrochem. Soc. 118 (1971) 1398.
[17] H. Nafe, J. Appl. Electrochem. 31 (2001) 1235.
[18] R. Singh, K.T. Jacob, J. Appl. Electrochem. 33 (2003) 571.
[19] C. Wanger, Z. Phys. Chem. B21 (1933) 25.
[20] A. Mineshige, T. Taji, Y. Muroi, M. Kobune, S. Fukii, N. Nishi, M. Inaba, Z. Ogumi, Solid State Ionics 135 (2000) 481.
[21] H.-T. Lim, A.V. Virkar, J. Power Sources 180 (2008) 92.
[22] M.H. Hebb, J. Chem. Phys. 20 (1952) 185.
[23] A.V. Virkar, J. Power Sources 147 (2005) 8.
[24] A.V. Virkar, J. Power Sources 172 (2007) 713.
[25] A.V. Virkar, J. Nachlas, A.V. Joshi, J. Diamond, J. Am. Ceram. Soc. 73 (1990) 3382.